Reactive diffusion and stresses in spherical geometry

Z. Erdélyi [a],[*], G. Schmitz [b]

[a] *Department of Solid State Physics, University of Debrecen, P.O. Box 2, H-4010 Debrecen, Hungary*
[b] *Institute of Material Physics, Westf. Wilhelms-Universität, Wilhelm-Klemm-Str. 10, 48149 Münster, Germany*

Abstract

We present an analytical model to calculate development of stress and plastic relaxation during reactive diffusion in core shell nano-structures. The complex model can be considered as a Stephenson's model [Acta Metal 1988;36:2663] on spherical geometry. Using our derivation, however, even the original equations for the planar case may be deduced in an easier way than in the original work by Stephenson. We apply the model to the reaction in spherical triple layers $A/B/A$ and $B/A/B$, for which Schmitz et al. [Acta Mater 2009;57:2673] observed by atom probe tomography that growth rate depends on the stacking order. Comparison with experimental data proves that significant deviations from vacancy equilibrium appear which control the stability and reaction rate of the nanometric diffusion couples.

© 2011 Acta Materialia Inc. Published by Elsevier Ltd. All rights reserved.

Keywords: Stress; Anisotropic stress relaxation; Spherical geometry; Reactive diffusion; Core shell

1. Introduction

The interdependence of interdiffusion and stress is a delicate problem. Imbalanced currents and different partial volumes of the diffusing species, and in the case of reactive diffusion also a possible excess volume of the product, may influence local stress [1]. One of the first trials to treat the problem was carried out by Larché and Cahn [2,3]. The first complete set of differential equations including the minimum set of required basic phenomena was, however, given by Stephenson [4]. His model, for planar geometry, included equations to calculate diffusion flux and corresponding change in composition, together with stress developing due to the imbalanced currents and different partial volumes, and also stress relaxation by plastic deformation. Nevertheless, the interdependence of diffusion and stress is still a challenging problem owing to its complexity [5–8].

Reactive diffusion on the nanoscale has become very important in spherical geometry since 2004. Numerous papers on hollow nanoshell formation have been published (e.g. [9–15]). Metallic spheres were reacted with oxygen and sulfur to produce nanoshells of oxides or sulfides. Also, nanoshell formation by pure interdiffusion was shown in Ref. [16]. In these reactions, the role of stresses has not been clarified, although in the case of closed geometries and large curvature they must play a significant role.

Moreover, Schmitz et al. [17] investigated by atom probe tomography (APT) the reaction of Al/Cu/Al and Cu/Al/Cu triple layers on the top of a tip of 25 nm apex radius (for illustration see Fig. 1). They showed that the growth rate of intermetallic products can depend significantly on the stacking order of the diffusion couples. This asymmetry in growth is very probably due to stress effects. Using an ad hoc layer model that postulated a physically reasonable stress relaxation inside the growing product, Schmitz et al. [17] predicted that compressive stress develops in the center of a spherical geometry. Without detailed justification, it was proposed that this inhomogeneous stress requires a transition from a fast Darken to a slow

* Corresponding author.
 E-mail address: zerdelyi@dragon.unideb.hu (Z. Erdélyi).
 URL: http://dragon.unideb.hu/~zerdelyi (Z. Erdélyi).
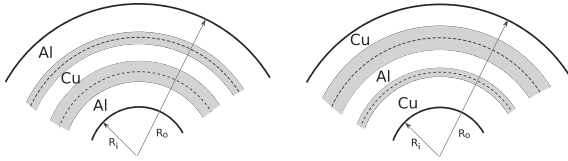
Fig. 1. Scheme of Al/Cu/Al and Cu/Al/Cu triple layers on top of a tip of R_i apex radius. The shaded stripes show the Al$_2$Cu intermetallics grown asymmetrically, depending on the stacking. The dashed lines indicates the initial interfaces.

Nernst–Planck interdiffusion regime, dependent on the stacking order.

These recent observations and propositions show that a rigorous model of reactive diffusion in spherical geometries of high curvature which considers stress and plastic relaxation without ad hoc assumptions would be highly desirable. In particular, the role of vacancies and the proposed switching between the two interdiffusion regimes must be elucidated from the theoretical side, since vacancy densities and flows cannot be measured directly. In this article such a model is developed on the basis of continuous analytical differential equations and applied to core shell geometries.

2. Basic equations

In equilibrium the internal stresses in every volume element must balance. Thus the equations of equilibrium for a deformed body are[1] [18]

$$\frac{\partial \sigma_{ik}}{\partial x_k} = 0 \tag{1}$$

where x_k is the spacial coordinate and σ_{ik} is the stress tensor, which is given in the case of isotropic elasticity by

$$\sigma_{ik} = \frac{E}{(1+v)(1-2v)}[(1-2v)\varepsilon_{ik} + v\varepsilon_{ll}\delta_{ik}] \tag{2}$$

Here, E is Young's modulus, v is Poisson's ratio, δ_{ik} is the unit tensor and ε_{ik} is the strain tensor. For small deformations, the strain tensor is given by

$$\varepsilon_{ik} = \frac{1}{2}\left(\frac{\partial u_i}{\partial x_k} + \frac{\partial u_k}{\partial x_i}\right) \tag{3}$$

u_i is the displacement vector.

Combining Eqs. (1)–(3), we can express the equation of equilibrium in terms of the displacement vector:

$$2(1-v)\text{grad div}\vec{u} - (1-2v)\text{ rot rot}\vec{u} = 0 \tag{4}$$

which is a particularly useful form to determine the shape of a body under external forces.

---

[1] In accordance with the usual role, we omit the sign of summation over vector and tensor suffixes. Summation over the values 1, 2, 3 is understood with respect to all suffixes which appear twice in the given term.

3. Equation of equilibrium in the case of internal stress-free strain

Eqs. (1)–(4) cannot be applied when the body is deformed by internal forces. For example, in interdiffusion, the transported net volume is usually not zero; accordingly, volume elements of a body expand or contract. In the case of solid-state reaction, even excess volume may be required by the reaction product. As such an expansion in general cannot proceed freely in a continuous body, stresses are set up.

In order to consider the deformation caused by internal changes, an extra term has to be included in Eq. (2), since the total strain (ε_{ik}) is not equal to the elastic strain (ε_{ik}^E) but $\varepsilon_{ik} = \varepsilon_{ik}^E + \omega_{ik}$, where ω_{ik} is the strain caused by the internal changes, such as stress-free expansion and plastic relaxation. Accordingly, Eq. (2) becomes

$$\sigma_{ik} = \frac{E}{(1+v)(1-2v)}\{[(1-2v)\varepsilon_{ik} + v\varepsilon_{ll}\delta_{ik}] - [(1-2v)\omega_{ik} + v\omega_{ll}\delta_{ik}]\} \tag{5}$$

As above, by combining Eqs. (1), (2) and (5) we get the general form of the equation of equilibrium in terms of the displacement vector:

$$2(1-v)\text{grad div}\vec{u} - (1-2v)\text{ rot rot }\vec{u} = 2(1-v)\text{ div }\hat{\omega} + 2v\text{grad tr}\hat{\omega} \tag{6}$$

where tr$\hat{\omega}$ denotes the trace of the tensor $\hat{\omega}$.

As we have not imposed any restriction on the tensors $\hat{\varepsilon}$ and $\hat{\omega}$, Eq. (6) is valid for any kind of deformation, whether isotropic or anisotropic.

As stress-free expansion and plastic deformation are considered in our model, $\omega_{ik} = \varepsilon_{ik}^{SF} + \varepsilon_{ik}^P$. Stress-free expansion is supposed to be isotropic; accordingly, it has the form $\varepsilon_{ik}^{SF} = \varepsilon^{SF}\delta_{ik}$. In plastic deformation, the volume remains constant, i.e. tr$\hat{\varepsilon}^P = 0$; in other words, plastic deformation is anisotropic. It can be supposed, however, that all the non-diagonal elements of the tensor $\hat{\varepsilon}^P$ are equal to zero; therefore, its components can be expressed as $\varepsilon_{ik}^P = \varepsilon_{ik}^P\delta_{ik}$. Thus,

$$\sigma_{ik} = \frac{E}{(1+v)(1-2v)}\{[(1-2v)\varepsilon_{ik} + v\varepsilon_{ll}\delta_{ik}] - [(1+v)\varepsilon^{SF} + (1-2v)\varepsilon_{ik}^P]\delta_{ik}\} \tag{7}$$

and the equation of equilibrium (6) now reads:

$$\frac{1-v}{1+v}\text{grad div}\vec{u} - \frac{1-2v}{2(1+v)}\text{rot rot}\vec{u} = \text{grad}\varepsilon^{SF} + \frac{1-2v}{1+v}\text{div}\hat{\varepsilon}^P \tag{8}$$

Further details on plastic strain are given in Section 6.

4. Solution of the equation of equilibrium

In this section, we present the solution of Eq. (8) for spherical geometry (for planar geometry see Section A.1). We deduce the components of the stress tensor and the displacement vector, since they are needed in the following to solve the correct diffusion equations.

Supposing spherical symmetry of the problem, only u_r differs from zero. Moreover, since $\varepsilon^P_{\Theta\Theta} = \varepsilon^P_{\phi\phi}$ in spherical geometry, Eq. (8) has the following form in spherical coordinates:

$$\frac{1-v}{1+v}\frac{d}{dr}\left[\frac{1}{r^2}\frac{d(r^2 u)}{dr}\right] = \frac{d\varepsilon^{SF}}{dr}$$
$$+ \frac{1-2v}{1+v}\left[\frac{d\varepsilon^P_{rr}}{dr} + \frac{2}{r}\left(\varepsilon^P_{rr} - \varepsilon^P_{\Theta\Theta}\right)\right] \quad (9)$$

Its solution is

$$u = \frac{1+v}{1-v}\frac{1}{r^2}\int_{R_i}^r r^2\left[\varepsilon^{SF} + \frac{1-2v}{1+v}\left(\varepsilon^P_{rr} + A\right)\right]dr + C_1 r + \frac{C_2}{r^2} \quad (10)$$

where

$$A = 3\int_{R_i}^r \frac{\varepsilon^P_{rr}}{r}\,dr \quad (11)$$

Furthermore, we made use of $\varepsilon^P_{rr} = -2\varepsilon^P_{\Theta\Theta}$, since $\varepsilon^P_{\Theta\Theta} = \varepsilon^P_{\phi\phi}$ and $\mathrm{tr}\,\hat{\varepsilon}^P = 0$. C_1 and C_2 are constants of integration to be determined from boundary conditions and R_i is any convenient lower limit for the integral, such as the inner radius of a hollow sphere, or $R_i = 0$ for a solid sphere.

The components of the total strain tensor in the spherical coordinates are $\varepsilon_{rr} = du/dr$ and $\varepsilon_{\Theta\Theta} = u/r$ [18]. For these, we obtain

$$\varepsilon_{rr} = \frac{du}{dr} = -\frac{2}{r^3}\frac{1+v}{1-v}\left\{\int_{R_i}^r r^2\left[\varepsilon^{SF} + \frac{1-2v}{1+v}\left(\varepsilon^P_{rr} + A\right)\right]dr\right.$$
$$\left. + \varepsilon^{SF} + \frac{1-2v}{1+v}\left(\varepsilon^P_{rr} + A\right)\right\} + C_1 - \frac{2C_2}{r^3},$$
$$\varepsilon_{\Theta\Theta} = \frac{1+v}{1-v}\frac{1}{r^3}\int_{R_i}^r r^2\left[\varepsilon^{SF} + \frac{1-2v}{1+v}\left(\varepsilon^P_{rr} + A\right)\right]dr + C_1$$
$$+ \frac{C_2}{r^3} \quad (12)$$

The components of the stress tensor are determined by substituting strains into Eq. (7):

$$\sigma_{rr} = -\frac{2E}{1-v}\frac{1}{r^3}\int_{R_i}^r r^2\left[\varepsilon^{SF} + \frac{1-2v}{1+v}\left(\varepsilon^P_{rr} + A\right)\right]dr + \frac{E}{1+v}A$$
$$+ \frac{E}{1-2v}C_1 - \frac{2E}{1+v}\frac{C_2}{r^3},$$

$$\sigma_{\theta\theta} = \sigma_{\phi\phi}$$
$$= \frac{E}{1-v}\frac{1}{r^3}\int_{R_i}^r r^2\left[\varepsilon^{SF} + \frac{1-2v}{1+v}\left(\varepsilon^P_{rr} + A\right)\right]dr$$
$$- \frac{E}{1-v}\left(\varepsilon^{SF} - \frac{\varepsilon^P_{rr}}{2} - \frac{v}{1+v}A\right) + \frac{E}{1-2v}C_1$$
$$+ \frac{E}{1+v}\frac{C_2}{r^3} \quad (13)$$

4.1. Hollow sphere – rigid inner and free outer surfaces

If the inner surface is rigid, we have for the displacement there: $u(R_i) = 0$. Thus, it follows from Eq. (10) that

$$C_2 = -C_1 R_i^3 \quad (14)$$

Moreover, the sphere is free to expand in radial direction, which means that the radial component of the stress tensor vanishes at the outer surface: $\sigma_{rr}(R_o) = 0$, where R_o denotes the radius of the outer surface of the sphere. Combining this boundary condition with Eqs. (13) and (14), we obtain the following expression for C_1:

$$C_1 = \frac{2}{1-v}\frac{(1+v)(1-2v)}{(1+v)R_o^3 + 2(1-2v)R_i^3}$$
$$\times \int_{R_i}^{R_o} r^2\left[\varepsilon^{SF} + \frac{1-2v}{1+v}\left(\varepsilon^P_{rr} + A\right)\right]dr$$
$$- \frac{1-2v}{(1+v)R_o^3 + 2(1-2v)R_i^3}A(R_o)R_o^3 \quad (15)$$

4.2. Hollow sphere – free inner and outer surfaces

If both the inner and outer surfaces are free to expand, the radial component of the stress tensor vanishes at outer and inner surfaces as well; that is, $\sigma_{rr}(R_i) = 0$ and $\sigma_{rr}(R_o) = 0$. Substituting the first boundary condition into Eq. (7), we obtain the following relation between C_1 and C_2:

$$C_2 = \frac{1+v}{2(1-2v)}R_i^3 C_1 \quad (16)$$

Then, combining the second boundary condition, Eq. (13) and relation (16), C_1 can finally be determined:

$$C_1 = 2\frac{1-2v}{1-v}\frac{1}{R_o^3 - R_i^3}$$
$$\times \int_{R_i}^{R_o} r^2\left[\varepsilon^{SF} + \frac{1-2v}{1+v}\left(\varepsilon^P_{rr} + A\right)\right]dr - \frac{1-2v}{1+v}$$
$$\times \frac{R_o^3}{R_o^3 - R_i^3}A(R_o) \quad (17)$$

5. Stress-free volume change ($\hat{\varepsilon}^{SF}$)

The above theory is quite general. It can be used for any kind of internal stress-free volume change and plastic relaxation. In the following, we will describe how ε^{SF} can be determined in diffusive solid state reaction.

In general, it is necessary to distinguish between transport by diffusion and transport by deformation (convection) caused by an imbalance in partial diffusional fluxes, the creation/annihilation of vacancies and the change in specific volume caused by reaction. The total flux of each chemical component relative to the fixed spatial coordinate system (laboratory frame of reference) can be written as the sum of diffusive and convective terms [19,4]:

$$\vec{j}_i^{\,0} = \vec{j}_i + \rho_i \vec{v} \quad \text{for } i = 1,\ldots,n \text{ and } i = v \quad (18)$$

where $\vec{j}_i$ and ρ_i are the diffusive flux and the density of component i, respectively, and $\vec{v}$ is the local material

velocity (in fact, the time derivative of the $\vec{u}$ displacement vector). Thus, in a coordinate system imagined as being embedded and deforming with the solid – called the material coordinate system – there is only diffusive transport. For this reason, calculation of the stress-free change of a volume element will be more convenient in the material coordinate system.

To calculate the rate of the stress-free volume change, we have to consider (i) the number of atoms and vacancies coming into and going out from a volume element, (ii) the number of vacancies created/annihilated and (iii) the change in specific volume with time. The first can be calculated from the total volume flux across the closed surface A, whereas (ii) and (iii) together can be considered as a sink/source term Q:

$$\frac{D\Delta V^{SF}}{Dt} = -\sum_{i=1}^{n} \oint_A (\Omega_i - \Omega_v)\vec{j_i}\,\vec{dA} + Q \tag{19}$$

where D/Dt is known as the substantial (or material) derivative. It gives the rate change of any scalar quantity seen at a point which follows the motion of the material coordinate system. It is related to the time derivative in the spatial coordinate system by $Da/Dt = \partial a/\partial t + \vec{v}\nabla a$. Moreover ΔV^{SF} is the stress-free change in the volume element, Ω_i is the atomic volume of component i and Ω_v is the volume of a vacancy. Note that, for a vacancy mechanism of diffusion, if an i species leaves the given volume, a vacancy enters, which explains $\Omega_i - \Omega_v$ in Eq. (19).

Applying Gauss's divergence theorem to Eq. (19), dividing each side of this equation by V (initial volume of the volume element) and taking $\lim_{V\to 0}$ leads to

$$\frac{D\varepsilon_{ll}^{SF}}{Dt} = -\sum_{i=1}^{n} \nabla'\left[(\Omega_i - \Omega_v)\vec{j_i}\right] + q \tag{20}$$

Here, ∇' indicates the divergence calculated in the material coordinate system and $q = \lim_{V\to 0} Q/V$ is the relative change in volume caused by creation/annihilation of vacancies and change in specific volume.

By definition, $\varepsilon^{SF} = \frac{1}{3}\varepsilon_{ll}^{SF}$; accordingly, we find for spherical geometry (for planar geometry see Appendix A.3)

$$\frac{D\varepsilon^{SF}}{Dt} = -\frac{1}{3}\left\{\frac{1}{r'^2}\sum_{i=1}^{n}\frac{\partial}{\partial r'}\left[r'^2(\Omega_i - \Omega_v)j_i\right] - q\right\} \tag{21}$$

since fluxes flow only in radial direction. By integration of this equation, ε^{SF} can be calculated at any time.

5.1. Fluxes

The flux of component i can be written as [4]

$$\vec{j_i} = -M_i\rho_i\nabla'\left[\left(\mu_i^{SF} + \Omega_i P\right) - \left(\mu_v^{SF} + \Omega_v P\right)\right] \quad \text{for } i$$
$$= 1,\ldots,n \tag{22}$$

where M_i denotes the mobility, ∇' indicates the gradient calculated in the material coordinate system, μ_i^{SF} and μ_v^{SF} are chemical potentials of component i and of the vacancy

in the stress-free state, respectively, and P is the pressure. This equation can also be written as

$$\vec{j_i} = -\rho\mathcal{D}_i\left\{\Theta_i c_v\nabla'c_i - \Theta_v c_i\nabla'c_v + \frac{c_i c_v}{RT}\nabla'[(\Omega_i - \Omega_v)P]\right\},$$
$$\text{for } i = 1,\ldots,n \tag{23}$$

where $\rho = \sum_{i=1}^{n}\rho_i + \rho_v$ is the total material density, c_i and c_v are the atomic fractions of component i and of the vacancy defined by

$$c_i = \frac{\rho_i}{\rho} \qquad \text{for } i = 1,\ldots,n \quad \text{and} \quad i = v \tag{24}$$

and Θ_i are appropriate thermodynamic factors [20]. Moreover, we conveniently define $\mathcal{D}_i = D_i^*/c_v$, where $D_i^* = M_i RT$ (for $i = 1,\ldots,n$) is the tracer diffusion coefficient of chemical component i [4,20].

The average density ρ can also be expressed in terms of partial atomic volumes:

$$\rho = \frac{1}{\sum_{i=1}^{n}c_i\Omega_i + c_v\Omega_v} \tag{25}$$

5.2. Thermodynamic factor

In order to model formation of a new phase during solid state reaction, the thermodynamic factors have to be chosen properly in Eq. (23).

A simple and straightforward way to determine Θ_i as a function of composition is to calculate the Gibbs energies of both the solid solution phase and that of the intermetallic. From the Gibbs energies, phase stabilities can be determined, and corresponding chemical potentials are calculated. The thermodynamic factors are then obtained by

$$\Theta_i = \frac{1}{RT}\frac{d\mu_i}{d\ln c_i} \tag{26}$$

In the following, we perform the calculation for a binary system. For the sake of simplicity, we model the formation of an intermetallic phase that is in equilibrium with ideal solid solutions.

The Gibbs energy of mixing of an ideal binary solid solution (SS) is natural, while the Gibbs energy of the intermetallic phase (IM) may be approximated by a second-order polynomial,

$$g^{SS} = RT[c\ln c + (1-c)\ln(1-c)],$$
$$g^{IM} = -g_0 + V(c - c_m)^2 \tag{27}$$

Here, c is the atomic fraction of component A, c_m is the stoichiometric concentration of component A in the intermetallic phase, and g_0 and V are parameters by which the existence range of the intermetallic phase can be adjusted. Fig. 2 presents these Gibbs energies of mixing and a corresponding composition profile.

With this, the chemical potentials of component A for the solid solution and the intermetallic phases are
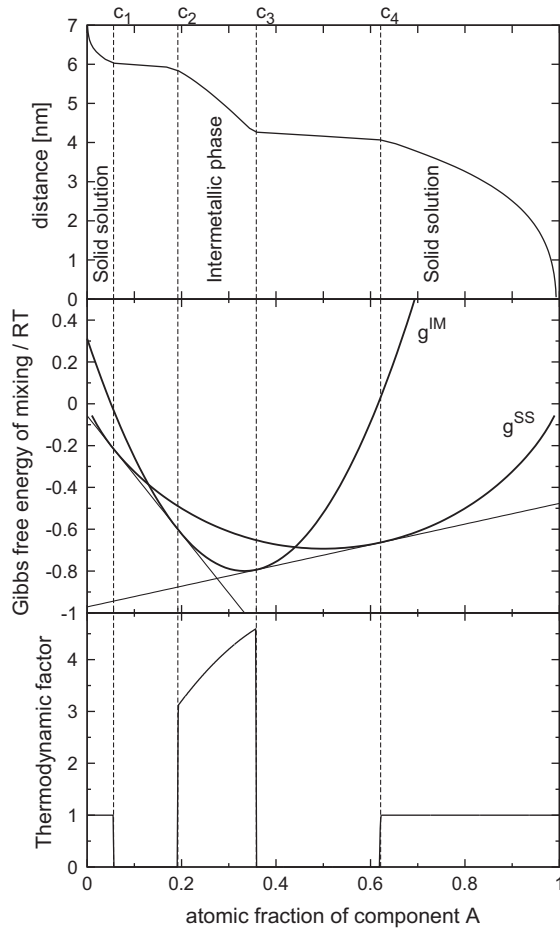
Fig. 2. The middle panel shows the Gibbs energy of mixing for a solid solution (g^{SS}) and an AB_2 intermetallic (g^{IM}) phases; the top panel illustrates the corresponding composition profile calculated for planar geometry ignoring all stress effects; the bottom panel demonstrates the thermodynamic factor vs. composition. c_1–c_4 are compositions of the phase boundaries ($c_m = 0.33333$, $g_0/RT = 0.8$ and $V/RT = 10$).

$$\mu_A^{SS} = RT \ln c, \quad \mu_A^{IM} = -g_0 + V\left(-c^2 + c_m^2 + 2c - 2c_m\right) \qquad (28)$$

As in the composition range $0 - c_1$, $g^{SS} < g^{IM}$, the thermodynamic factor is calculated from μ_A^{SS}; in the range $c_2 - c_3$, $g^{IM} < g^{SS}$, thus Θ_A (which is equal to Θ_B in a binary system) is calculated from μ_A^{IM}; and in the range $c_4 - 1$, it is calculated again from μ_A^{SS}. In the two-phase ranges $c_1 - c_2$ and $c_3 - c_4$, the chemical potential remains constant (equal to $\mu_A(c_1)$ and $\mu_A(c_3)$), which results in vanishing thermodynamic factors. This variation of the thermodynamic factor with composition calculated from Eq. (26) is also presented in Fig. 2.

5.3. Continuity equation

Considering that the vacancy density changes not only due to atomic fluxes, but also due to the activity of sinks and sources for vacancies, the continuity equations in the material coordinate system are

$$\frac{D\rho_i}{Dt} = -\nabla' \overrightarrow{j_i} \quad \text{for } i = 1, \ldots, n;$$

$$\frac{D\rho_v}{Dt} = -\nabla' \overrightarrow{j_v} + S_v \qquad (29)$$

Here, S_v is a vacancy source term, i.e. the number of vacancies created in unit volume per unit time, and relates to q by

$$q = S_v \Omega_v \qquad (30)$$

Summing Eq. (29) and regarding that the total material density is $\rho = \sum_{i=1}^{n} \rho_i + \rho_v$ and $\sum_{i=1}^{n} \overrightarrow{j_i} = -\overrightarrow{j_v}$ leads to

$$\frac{D\rho}{Dt} = S_v \qquad (31)$$

It is often more convenient to use atomic fractions instead of material density. By differentiating Eq. (24), we obtain

$$\frac{Dc_i}{Dt} = \frac{1}{\rho}\frac{D\rho_i}{Dt} - \frac{c_i}{\rho}\frac{D\rho}{Dt} \quad \text{for } i = 1, \ldots, n \qquad (32)$$

Using Eqs. (29) and (31), Eq. (32) takes the form

$$\frac{Dc_i}{Dt} = -\frac{1}{\rho}\nabla' \overrightarrow{j_i} - c_i \frac{S_v}{\rho} \qquad (33)$$

The ratio S_v/ρ gives the rate of changing the atomic fraction of vacancies due to creation/annihilation. Abbreviating

$$s_v = \frac{S_v}{\rho} \qquad (34)$$

we finally get the following form:

$$\frac{Dc_i}{Dt} = -\frac{1}{\rho}\nabla' \overrightarrow{j_i} - c_i s_v \qquad (35)$$

which has the following form for spherical geometry if fluxes flow only in radial direction:

$$\frac{Dc_i}{Dt} = -\frac{1}{\rho r'^2}\frac{\partial}{\partial r'}[r'^2 j_i] - c_i s_v \qquad (36)$$

5.4. Sinks and sources – q

As was written above, we consider two contributions to q: the relative change in volume caused by creation/annihilation of vacancies (q_v) and the change in specific volume (q_{sv}):

$$q = q_v + q_{sv} \qquad (37)$$

It is reasonable to suppose that a pressure $P(= -\frac{1}{3}\mathrm{tr}\hat{\sigma})$ modifies the stress-free equilibrium atomic fraction of vacancies c_v^0 to

$$c_v(P) = c_v^0 \exp\left(-\frac{\Omega_v P}{RT}\right) \qquad (38)$$

The rate of creation/annihilation of vacancies is proportional to the deviation of the current fraction of vacancies from its equilibrium value

$$s_v = K_r \left[c_v^0 \exp\left(-\frac{\Omega_v P}{RT} \pm \frac{L}{R_{i/o}}\right) - c_v \right] \qquad (39)$$

where the rate coefficient K_r determines the effectiveness of sinks and sources. Therefore s_v gives the rate change of the

fraction of vacancies. We emphasize that K_r is not necessarily a constant but may vary, for instance, with spatial coordinates, depending on the spatial distribution of the sinks and sources. Moreover, the equilibrium vacancy concentration at the inner boundary of a hollow sphere is higher than at a flat surface $\left(c_v(R_i) = c_v^0 e^{L/R_i}\right)$ while lower at the outer boundary $\left(c_v(R_o) = c_v^0 e^{-L/R_o}\right)$ due to the Gibbs–Thomson effect. $L = 2\gamma\Omega_v/RT$, and γ is the surface tension.

Using the relations (30) and (34), the contribution of the creation/annihilation of vacancies to q is

$$q_v = s_v \rho \Omega_v \tag{40}$$

The relative change q_{sv} in volume due to phase transformation represents an input parameter. For example, if the change in specific volume for a reaction $A + B \rightarrow AB$ is 6%, then $q_{sv} = 0.06$.

6. Plastic deformation $(\hat{\varepsilon}^P)$ – stress relaxation

Plastic deformation is a well-known mechanism of stress relaxation, which is governed by the shear part of the stress tensor. Only shear (deviatoric) stress $(\hat{\sigma}^{shear})$ induces shear strain $(\hat{\varepsilon}^p)$ or strain rate $\left(\dot{\hat{\varepsilon}}^p\right)$ – superscript "p" means plastic in our case. When large plastic deformation occurs, then the distribution of shear stress is determined, for example, by viscous flow, viz. $\hat{\sigma}^{shear} = 2\eta\dot{\hat{\varepsilon}}^p$, where η is the shear viscosity. This follows from the definition of η. Accordingly,

$$\dot{\hat{\varepsilon}}^p = \frac{1}{2\eta}\hat{\sigma}^{shear} = \frac{1}{2\eta}\left(\hat{\sigma} - \frac{1}{3}\mathrm{tr}\hat{\sigma}\right) \tag{41}$$

In particular, for spherical geometry (for planar geometry see Appendix A.3)

$$\dot{\varepsilon}_{rr}^P = \frac{1}{3\eta}(\sigma_{rr} - \sigma_{\Theta\Theta}), \quad \dot{\varepsilon}_{\Theta\Theta}^P = \dot{\varepsilon}_{\phi\phi}^p = -\frac{1}{6\eta}(\sigma_{rr} - \sigma_{\Theta\Theta}) \tag{42}$$

Other mechanisms besides viscous flow can lead to stress relaxation. Accordingly, Eq. (41) may be modified to calculate the strain rate as appropriate for the corresponding mechanism.

7. Calculation

To calculate the time evolution of radial composition and stress profiles, we need to solve a system of partial differential equations: basically Eqs. (36) and (13), with Eqs. (23), (34), (21) and (42). For this purpose, we used a finite volume method. The sample was divided into n spherical shells (slabs for planar geometry). In each computation cycle, the total number and volume of atoms transported between neighboring shells were calculated, from which the change of composition and stress in the shells were determined, together with their change in thickness.

In most cases, samples were divided into 120 shells; however, different numbers were also used to check the independency of the mesh.

For details of the algorithm and used input parameters, see Appendix C.

8. Results and discussion

8.1. Stress and plastic relaxation

In Ref. [17] reaction-induced stress was calculated by modeling a discrete triple layer. Ad hoc, it was proposed that, due to relaxation or creep in the growing layer, nature controls the aspect ratio between stress-free expansions in radial and azimuthal directions by minimization of elastic energy. Therefore, to test our equations deduced for the components of the stress tensor, including anisotropic relaxation, but also to verify the previous ad hoc assumption, we first calculated the stress in a trilayer system in close correspondence to the case reported in Fig. 7 in Ref. [17]. We mimicked a (7.5 nm Cu layer)/(5 nm Al_2Cu)/(7.5 nm Al layer) system on a tip of 25 nm apex radius (i.e. rigid inner interface, $R_i = 25$ nm). First, we increased the specific volume of the intermetallic phase by 6% isotropically, i.e. we set $\varepsilon^{SF} = 0.06$. Then we let the stress relax by viscous flow only inside the reaction product. As demonstrated in Fig. 3, the result is in very good agreement with that in Ref. [17], although not identical. Slight differences originate from the fact that the stress-free strain was supposed to be homogeneous across the intermetallic layer in the simplified scheme used in Ref. [17], whereas our present calculation is free from this constraint. This also explains why hydrostatic stress in the intermetallic is not homogeneous anymore, in contrast to Ref. [17].

It is interesting to note that, before plastic relaxation, hydrostatic stress is constant in all the layers, while discontinuous steps appear at the interfaces. Moreover, hydrostatic stress is tensile ($\sigma_{hydrost} > 0$) and has the same level in the pure A and B layers, whereas it is compressive ($\sigma_{hydrost} < 0$) in the intermetallic layer. During plastic relaxation the stress profiles change significantly. The hydrostatic stress decreases dramatically in the inner metallic layer; it even changes from tensile to compressive. In the intermetallic layer, the radial and tangential stresses converge, and since strain is no more constant, the hydrostatic stress also becomes inhomogeneous. In the outer metallic layer, the hydrostatic stress becomes even more tensile.

Similar to the trilayer case, we repeated the calculations for the five-layer system, which was in fact the real experimental geometry. Fig. 4 demonstrates very good agreement with the results reported in Fig. 9 in [17], although they are not completely identical for similar reasons to those explained before. The radial and tangential stresses inside the intermetallic layers converge during relaxation and the hydrostatic stress decreases. As a consequence, stresses in the metallic layers become increasingly compressive towards the center of the geometry.

8.2. Reactive diffusion

We are now in a position to predict the influence of the stresses on the reactive diffusion. First, we show results obtained for reaction in spherical bilayers. Vacancy sinks
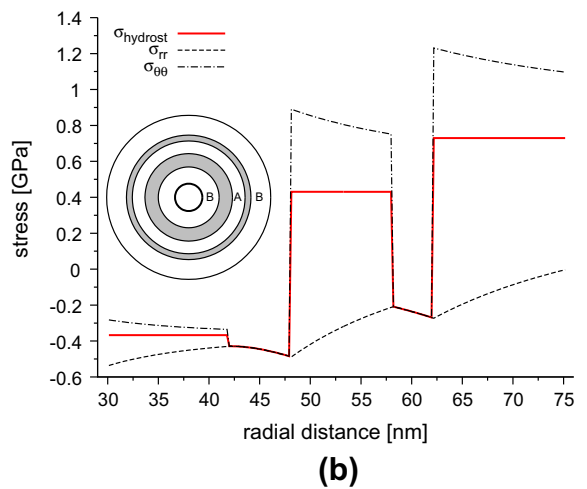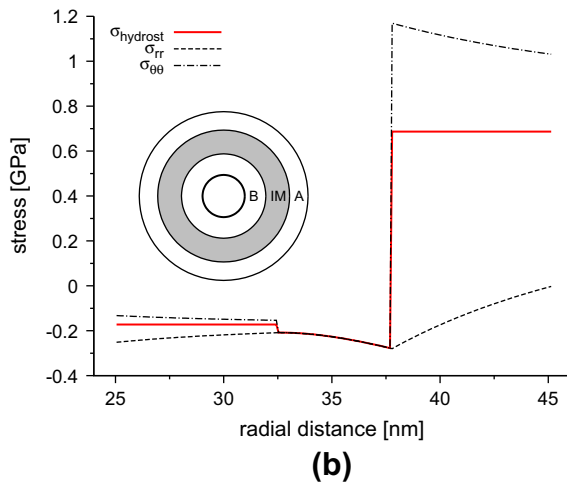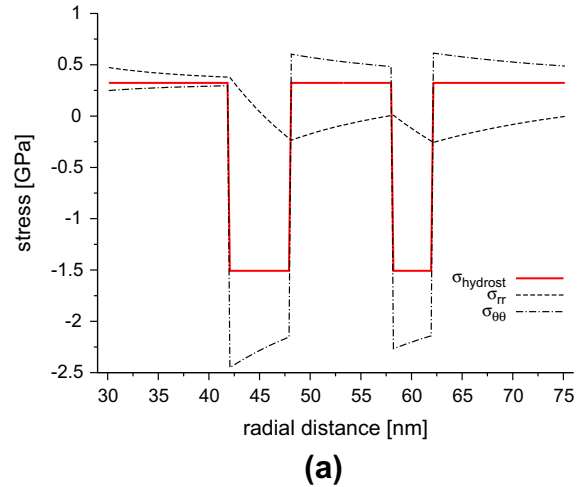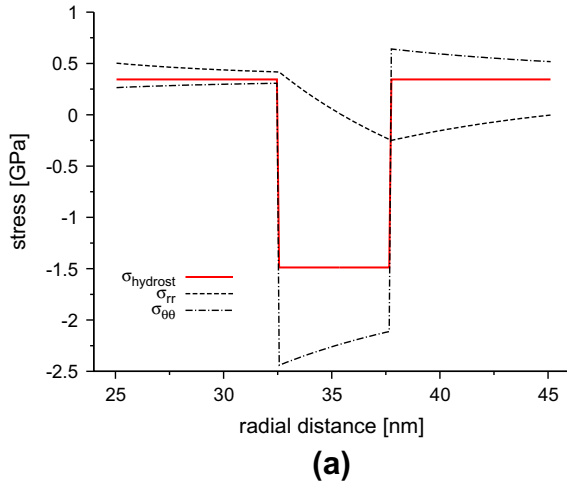
Fig. 3. Profile of radial, tangential and hydrostatic stresses produced by reaction-induced excess volume (curvature of substrate 25 nm, initial layer thickness of A and B 10 nm, thickness of reaction product 5 nm): (a) no relaxation; (b) complete relaxation. The inset shows a sketch of the geometry.

Fig. 4. Profiles of the radial, tangential and hydrostatic stresses produced by reaction-induced excess volume plotted vs. the distance to the center of a spherical geometry with an inner radius of 30 nm: (a) no relaxation and (b) complete relaxation.

and sources were supposed to be active only at the inner and outer surfaces of the structure, and in addition at the (presumably incoherent) interfaces of the metals to the growing intermetallic. At these positions $K_{eff} = 1$ was used (full efficiency of sinks and sources), whereas elsewhere $K_{eff} = 0$ (for a definition of K_{eff} see also Eqs. (39) and (57)). For simplicity, we neglected the Gibbs–Thomson effect, i.e. $L = 0$ was used.

To clarify the role of stress and possible relaxation, we performed the following concrete calculations for A/B (A is inside and B outside) and B/A stacking orders of the metals: (i) neglecting stress effects; (ii) taking into account stress development but neglecting plastic relaxation; and (iii) considering both stress development and plastic relaxation. In all calculations, partial diffusion coefficient of the majority component B inside the intermetallic (super-lattice structure) was 10 times higher than that of the A component. We obtained that in cases (i) and (ii) the thickness of the growing intermetallic layer was unaffected by the

stacking order. Fig. 5 illustrates that in case (iii), however, the growth rate of the intermetallic depends considerably on the layer stacking. For A/B stacking, the growth rate is depressed, whereas for B/A stacking, it is accelerated.

This asymmetry in growth rates in case (iii) is a consequence of the vacancy distribution produced by the different stress levels in the A and B matrixes. It is obvious that in cases (i) and (ii) vacancy concentration in both matrixes must be identical, since in case (i) stress effects are neglected and in case (ii), in the absence of plastic relaxation, the stress levels are the same in both the A and B matrixes (see also Fig. 3a). However, in case (iii) (Figs. 3b and 5b) there is tensile stress in the outer part of the sample and compressive stress in the inner part. Accordingly, the vacancy concentration increases in the outer part and decreases in the inner part. A gradient of vacancy concentration develops in the intermetallic layer which always points outwards, irrespectively of the stacking order. On the other hand, the direction of the vacancy flow, originating from the difference in

(a)

(b)
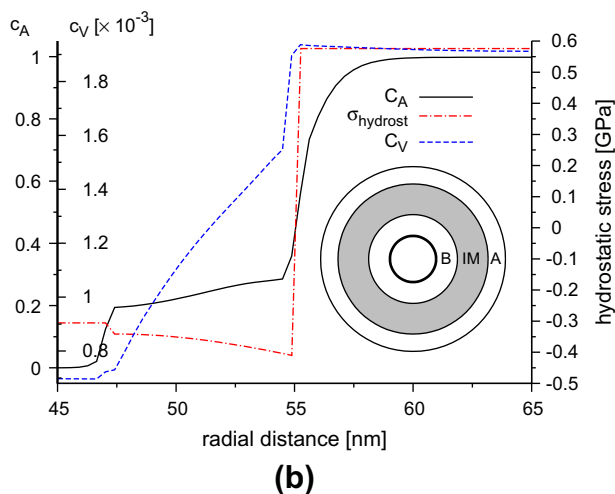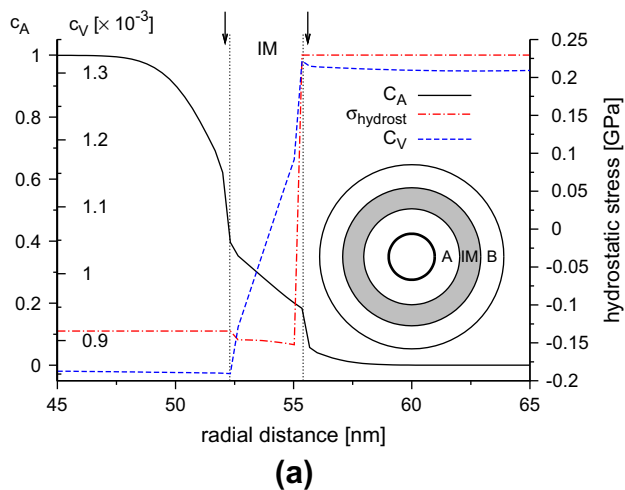
Fig. 5. Profiles of concentration of vacancies and *A* atoms as well as hydrostatic stress for (a) *A/B* and (b) *B/A* stacking. Both (a) and (b) correspond to the same diffusion time. The thicknesses of the intermetallics are (a) 2.3 and (b) 7.1 nm. ($R_i = 30$ nm, $R_o = 75$ nm, initial position of the interface at 52.5 mn.) Only the part around the intermetallics is shown. Vertical dotted lines mark the positions of interfaces, arrows those of sinks and sources of vacancies.

mobility of the *A* and *B* species, depends on the stacking order. It is always directed towards the *B* matrix. Thus, for *A/B* stacking, this resultant vacancy flow is directed up the gradient of vacancy concentration, while it is directed downwards for reversed stacking. In consequence, growth is hindered for *A/B* but accelerated for *B/A* stacking orders.

We also performed calculations for trilayered systems, in *A/B/A* and *B/A/B* stacking orders, to model the Cu/Al/Cu and Al/Cu/Al systems investigated by APT in Ref. [17]. We calculated the same three cases (i)–(iii) as for the bilayer. In cases (i) and (ii) the intermetallic layers grew at the same rate at the inner and outer reactive interfaces, whereas in case (iii) they grew at different rates (see Fig. 6).

On the basis of the explanation for the bilayer geometry, the interpretation of these results is quite straightforward. It is, again, the distribution of the vacancies determined

by the stress field that controls the growth rate. In case (iii) the profile of hydrostatic stress has a stepwise character, decreasing from outside to inside for both stacking orders. Accordingly, the vacancy concentration also decreases towards the center of the sphere. The intermetallic layer grows slower at the interface at which the direction of the gradient of vacancy concentration is opposite the gradient of the *A* (slower) atoms. As a result, the growth rate is larger at the outer interface for the *A/B/A* and at the inner interface for the *B/A/B* stacking.

In the extreme case, vacancy flow may become completely suppressed, if the gradient of vacancy concentration drives sufficiently against the expected (from the difference in atomic fluxes) transport direction of vacancies. Then both atomic species are forced to diffuse at an identical rate

(a)

(b)
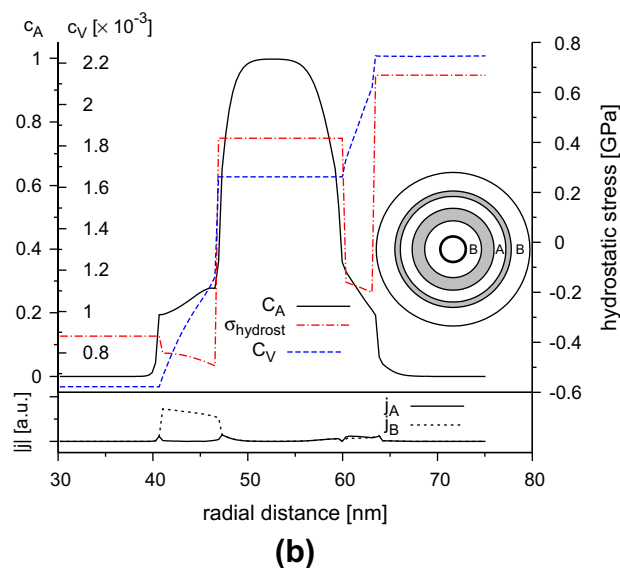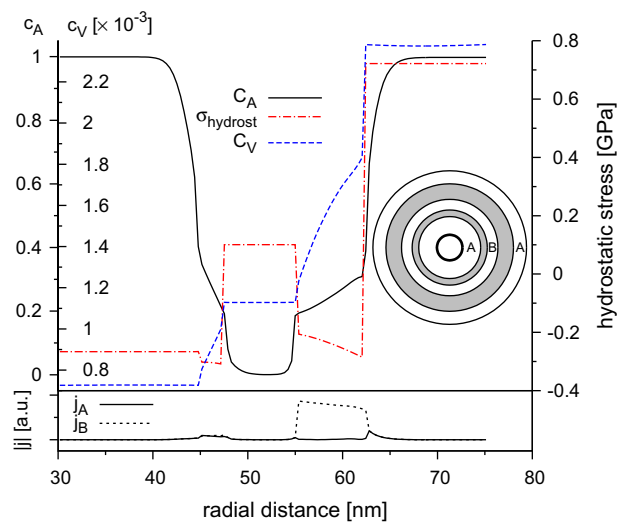
Fig. 6. Profiles of compositions of vacancies and *A* atoms, as well as hydrostatic stress (top panel), together with absolute values of partial fluxes (bottom panel) for (a) *A/B/A* and (b) *B/A/B* stacking orders. Both (a) and (b) correspond to the same time. ($R_i = 30$ nm, $R_o = 75$ nm.)

(though in opposite directions). This implication is confirmed by our detailed calculation. Fig. 6 (bottom panels) demonstrates that absolute values of the partial fluxes become practically equal across the intermetallic layer of slow growth, while across the intermetallic layer of fast growth, the flux of B atoms is considerably higher than that of A atoms. In this way, we may naturally interpret the different growth rates by transport in the Nernst–Planck (slow) or the Darken (fast) regime of interdiffusion, as was suggested in Ref. [17].

The derived model allows a detailed investigation of the role of distribution and the effectiveness of vacancy sinks and sources (vSS). To this end, we varied the efficiency of the sinks and sources K_{eff} at all inner interfaces from 1 down to 10^{-4}; only at the free (outer) surface was $K_{eff} = 1$ kept. The asymmetry in growth rates of the intermetallic products decreased with decreasing K_{eff}. It even disappeared for $K_{eff} = 10^{-4}$ and 10^{-2} for $A/B/A$ and $B/A/B$ stacking orders, respectively. We also performed the following calculations: (a) vSS only at the surfaces; (b) vSS distributed homogeneously; and (c) no vSS at all throughout the sample. In none of these cases did we observe significant growth asymmetry. Thus, the distribution of vSS is obviously a critical factor.

In reverse conclusion, the fact that a clear growth asymmetry was observed in the experiments demonstrates that in the nanometric devices very efficient sinks and sources are present at the interfaces of the intermetallic layers, while the newly build lattice structure within the intermetallic layer is so perfect that no vacancy relaxation could appear. In this way, the comparison with the presented theoretical study definitely proves that vacancy concentration in real nanometric diffusion couples deviates significantly from equilibrium during solid state reaction and that this makes a decisive impact on the reaction and stability of such devices.

We also investigated the role of the Gibbs–Thomson effect. However, we did not find any considerable effect for the studied curvature radii.

9. Conclusions

We have developed a complete set of analytical equations to describe reactive diffusion in spherical core shell nanostructures. The model takes into account elastic stress, its plastic relaxation, as well as possible non-equilibrium vacancy densities. Furthermore, thermodynamic driving forces are included to model formation of intermetallic product phases in intermediate composition range. The complex model can be considered as Stephenson's model for spherical geometry.

Using this model, we have managed to interpret observations reported in Ref. [17], namely that the growth rates of intermetallic products in metallic triple layers ($A/B/A$ and $B/A/B$) in spherical geometry depend on the stacking order. In the case of a positive excess volume of reaction, anisotropic relaxation of elastic stress leads to tensile hydrostatic stress in the outer shell but compressive stress in the center, independently of the stacking order. The inhomogeneous stress field induces an inhomogeneous distribution of vacancies. The resulting vacancy gradient provides an additional driving force that hinders the outward flux of vacancies. As a consequence, diffusion of the faster component towards the center can only proceed by slow Nernst–Planck interdiffusion instead of conventional fast Darken transport.

The model calculations provide evidence that the experimentally observed growth asymmetry can only appear if vacancy sinks and sources are present at the incoherent interphase boundaries but not within the formed intermetallic product layer.

The developed model will presumably also be useful in clarifying the role of stress in today's popular core shell nanostructures.

Appendix A. Planar geometry

A.1. Solution of the equation of equilibrium for planar geometry

In the case of a thin sample on a rigid substrate and one-dimensional (e.g. in x direction) variation of ε^{SF} – such as one-dimensional diffusion – only u_x differs from zero; that is, Eq. (8) has the following form:

$$\frac{1-v}{1+v}\frac{d^2 u_x}{dx^2} = \frac{d\varepsilon^{SF}}{dx} + \frac{1-2v}{1+v}\frac{d\varepsilon_{xx}^P}{dx} \tag{43}$$

Its solution is

$$u_x = \frac{1+v}{1-v}\int_0^x \left(\varepsilon^{SF} + \frac{1-2v}{1+v}\varepsilon_{xx}^P\right)dx + C_1 x + C_2 \tag{44}$$

where C_1 and C_2 are constants of integration to be determined from boundary conditions.

If the distance is measured from the top of the substrate, $u_x = 0$ at $x = 0$, and from Eq. (44) this requires that $C_2 = 0$. From Eqs. (3) and (44),

$$\varepsilon_{xx} = \frac{du_x}{dx} = \frac{1+v}{1-v}\varepsilon^{SF} + \frac{1-2v}{1-v}\varepsilon_{xx}^P + C_1,$$

$$\varepsilon_{yy} = \varepsilon_{zz} = \frac{du_y}{dy} = 0 \tag{45}$$

Substituting these expressions into Eq. (7), we get:

$$\sigma_{xx} = \frac{E}{(1+v)(1-2v)}(1-v)C_1 \quad (46)$$

As the sample is free to expand into the x direction, $\sigma_{xx} = 0$ anywhere, and it follows that $C_1 = 0$.

Therefore, the nonzero components of the displacement vector and the stress tensor (again from Eq. (7)) are

$$u_x = \frac{1+v}{1-v}\int_0^x \left(\varepsilon^{SF} + \frac{1-2v}{1+v}\varepsilon_{xx}^P\right)dx \quad (47a)$$

$$\sigma_{yy} = -\frac{E}{1-v}\left(\varepsilon^{SF} - \frac{\varepsilon_{xx}^P}{2}\right) \quad (47b)$$

A.2. ε^{SF} for planar geometry

For planar geometry, when fluxes flow in only one spatial direction, e.g. x,

$$\frac{D\varepsilon^{SF}}{Dt} = -\frac{1}{3}\left\{\sum_{i=1}^n \frac{\partial}{\partial x'}[(\Omega_i - \Omega_v)j_i] - q\right\} \quad (48)$$

A.3. $\hat{\varepsilon}^P$ (rate) for planar geometry

$$\dot{\varepsilon}_{xx}^P = -\frac{1}{3\eta}\sigma_{yy}, \quad \dot{\varepsilon}_{yy}^P = \dot{\varepsilon}_{zz}^P = \frac{1}{6\eta}\sigma_{yy} \quad (49)$$

Appendix B. Comparison to Stephenson's model

In this section, we show that, from our solution for planar geometry, the same equations can be deduced for stress development/relaxation and the drift velocity field as were obtained by Stephenson. Note that, for easier comparison with Stephenson's original formula, we use ∇ to denote the spatial derivation in the given direction.

As $P = -\frac{1}{3}\text{tr}\hat{\sigma}$, i.e. in this case $P = -\frac{2}{3}\sigma_{yy}$,

$$P = \frac{2}{3}\frac{E}{1-v}\left(\varepsilon^{SF} - \frac{\varepsilon_{xx}^P}{2}\right) \quad (50)$$

Moreover, deriving Eq. (50) by time and substituting $\dot{\varepsilon}_{xx}^P$ from Eq. (49), we obtain

$$\frac{DP}{Dt} = \frac{2}{3}\frac{E}{1-v}\left(\frac{D\varepsilon^{SF}}{Dt} + \frac{1}{6\eta}\sigma_{yy}\right) \quad (51)$$

Using again that $P = -\frac{2}{3}\sigma_{yy}$, $Y = E/(1-v)$ and considering Eq. (48),

$$\frac{DP}{Dt} = -\frac{2Y}{9}\left\{\sum_{i=1}^n \nabla[(\Omega_i - \Omega_v)j_i] - q\right\} - \frac{Y}{6\eta}P \quad (52)$$

which is equivalent to Stephenson's equation.

The gradient of the velocity field given by Stephenson in Ref. [21] can also be deduced. Deriving Eq. (44) by time and space, we get

$$\nabla v_x = \frac{1+v}{1-v}\left(\frac{D\varepsilon^{SF}}{Dt} + \frac{1-2v}{1+v}\dot{\varepsilon}_{xx}^P\right) \quad (53)$$

Substituting $\dot{\varepsilon}_{xx}^P$ from Eq. (49) into Eq. (53), we get

$$\nabla v_x = 3\frac{D\varepsilon^{SF}}{Dt} - 3(1-2v)\frac{2}{3}\frac{1}{(1-v)}\left(\frac{D\varepsilon^{SF}}{Dt} + \frac{1}{6\eta}\sigma_{yy}\right) \quad (54)$$

Substituting Eq. (48) into the first term of Eq. (54) and comparing the second term to Eq. (51), we obtain

$$\nabla v_x = -\sum_{i=1}^n \nabla[(\Omega_i - \Omega_v)j_i] + q - \frac{3(1-2v)}{E}\frac{DP}{Dt} \quad (55)$$

which is Stephenson's equation. Interestingly, the last term had not been included in Ref. [4]; it only appeared five years later, in Ref. [21].

We also note that the equations for spherical geometry and rigid inner interface are equivalent to the equations for planar geometry in the case of $R_i \to \infty$.

Appendix C. Algorithm and input parameters

Before starting the main calculation, we tabulate the thermodynamic factor on the basis of Section 5.2. The computational cycle of the main software then: (i) searches first for the value of the thermodynamic factor corresponding to the composition of each slab/shell; (ii) calculates the volume of a vacancy as the average atomic volume weighted by composition and multiplied by a scale factor K_v that takes into account volume relaxation by $\Omega_v = K_v \sum_{i=1}^n c_i\Omega_i / \sum_{i=1}^n c_i$ and determines the density based on Eq. (25); (iii) computes the values of $\mathcal{D}_i$ if they are composition dependent (e.g. $\mathcal{D}_i = \mathcal{D}_i^0 \exp(m_i c_i)$ [22], where m_i gives the strength of the composition dependence); (iv) determines the fluxes by Eq. (23); (v) determines the rate change of the atomic fraction of vacancies due to creation/annihilation by Eq. (57) (see below) (for planar geometry with $L = 0$); (vi) updates the composition according to Eq. (36) (for planar geometry Eq. (35)) with (25); (vii) calculates the stress-free strain by integrating Eq. (21) (Eq. (48) for planar geometry) with respect to time from zero to current time (using Eqs. (37) and (40)); (viii) deduces the tangential and radial components of the stress tensor from Eq. (13) with Eqs. (11) and (42), and the constants of integration for the desired case: Eqs. (15) and (14) for a rigid inner surface, Eqs. (17) and (16) for a free inner surface (the pressure from Eq. (52) for planar geometry) by integration with respect to time from zero to current time; and finally (ix) updates the position of the border of the slabs/shells according to Eq. (10) with Eqs. (11) and (42), and the constants of integration for the desired case: Eqs. (15) and (14) for a rigid inner surface, Eqs. (17) and (16) for a free inner surface (Eq. (47b) for planar).

Note that, for better stability of the algorithm, steps (v) and (vi) were realized in substeps. To calculate the composition at time $t + \Delta t$, first the change in composition due to diffusion was calculated, then the composition was updated by

$$c_i^* = c_i(t) + \frac{1}{\rho}\nabla' \vec{j_i}\,\Delta t, \quad \text{for } i = A, B$$
$$c_v = 1 - c_A^* - c_B^* \tag{56}$$

Here, c_i^* and c_v^* denote that the compositions do not attaine their desired values at time $t + \Delta t$. Note that ∇' is equal to $\frac{1}{r'^2}\frac{\partial}{\partial r'}(r'^2\ldots)$ for spherical and $\frac{\partial}{\partial x'}$ for planar geometry. Then the vacancy composition was equilibrated by

$$c_v(t + \Delta t) = c_v^* + s_v,$$
$$s_v = \frac{K_{eff}}{\Delta t}\left[c_v^0 \exp\left(-\frac{\Omega_v P}{RT}\right) - c_v^*\right] \tag{57}$$

where $0 \leqslant K_{eff} \leqslant 1$ determines the efficiency of the vacancy sinks and sources. Finally, the composition of the atoms was also updated as required:

$$c_i(t + \Delta t) = c_i^* - c_i^* s_v \Delta t, \quad \text{for } i = A, B \tag{58}$$

Note that the division by Δt in Eq. (57) is necessary because s_v is the change rate of c_v, and it is also used to calculate the stress-free strain in step (vii).

The following input parameters were used: R_i and R_o were in the range of 0–100 nm. Initially, the vacancies were distributed homogeneously. Usually $c_v^0 = 10^{-3}$ was used, although this is much larger than in real cases. For a realistic value of c_v^0, the computation time would have to have been increased significantly. For test purposes, in some cases $c_v^0 = 10^{-4}$–10^{-6} was used. From these calculations, we concluded that the value of c_v^0 did not change the results qualitatively. K_{eff}: $0 \leqslant K_{eff} \leqslant 1$ and $m_i = 0$ were used. $D_A^*/D_B^* = \mathcal{D}_A/\mathcal{D}_B = 0.1$ in the intermetallic phases; outside, $\mathcal{D}_A = \mathcal{D}_B$. These correspond to the suppositions in Ref. [17]. $\mathcal{D}_A = 1.8 \times 10^{-14}$ m^2 s^{-1}; however, its value does not play an important role, just scales the time. As we did not intend to fit experimental data, determination of the real time scale was not crucial. $\Omega_A = \Omega_B = 7 \times 10^{-6}$ m^3 mol^{-1} and $K_v = 1$ were applied. $T = 700$ K, although used in the calculations presented in this work, does not play any role, since, due to the supposition $\Omega_A = \Omega_B = \Omega_v$, the only term containing the temperature explicitly (see Eq. (23)) vanishes.

$E = 90$ GPa and $v = 0.345$ were supposed, just as in Ref. [17]. To mimic the conditions supposed in Ref. [17], the viscosity was set to 10^{100} Pa outside the intermetallic phases to prevent any relaxation, and to 10^3 Pa inside the intermetallic phases to allow complete plastic relaxation.

References

[1] Beke D, Szabó I, Erdélyi Z, Opposits G. Mater Sci Eng A 2004;387–389:4.
[2] Larché F, Cahn J. Acta Metal 1985;33:331.
[3] Larché F, Cahn J. Acta Metal 1982;30:1835.
[4] Stephenson GB. Acta Metal 1988;36(10):2663–83.
[5] Svoboda J, Fischer F. Acta Mater 2011;59:1212. and references therein.
[6] Fischer F, Svoboda J. Acta Mater 2010;58:2698. and references therein.
[7] Gusak A, Kornienko S, Lutsenko G. Def Diff Data 2007;264:109.
[8] Gusak A. Mater Sci Forum 1994;155–156:55.
[9] Yin Y, Rioux RM, Erdonmez CK, Cabot A, Hughes S, Alivisatos AP. Science 2004;304:711.
[10] Yin Y, Erdonmez CK, Cabot A, Hughes S, Alivisatos AP. Adv Funct Mater 2006;16:1389.
[11] Wang CM, Baer D, Thomas L, Amonette J, Antony J, Qiang Y, et al. J Appl Phys 2005;98:09430.
[12] Nakamura R, Lee JG, Tokozakura D, Mori H, Nakajima H. Mater Lett 2007;61:1060.
[13] Nakamura R, Tokozakura D, Nakajima H, Lee JG, Mori H. J Appl Phys 2007;101:074303.
[14] Nakamura R, Lee JG, Mori H, Nakajima H. Philos Mag 2008;88:257.
[15] Nakajima H, Nakamura R. J Nano Res 2009;7:1.
[16] Glodan G, Cserhati C, Beszeda I, Beke DL. Appl Phys Lett 2010;97:113109.
[17] Schmitz G, Ene CB, Nowak C. Acta Mater 2009;57(9):2673–83.
[18] Landau LD, Lifshitz EM. Theory of elasticity. Course of theoretical physics, 2nd ed., vol. 7. Pergamon Press; 1970.
[19] Philibert J. Atom movements: diffusion and mass transport in solids. Les Editions de Physique; 1991.
[20] Mehrer H. Diffusion in solids. Berlin/Heidelberg: Springer-Verlag; 2007.
[21] Stephenson GB. Def Diff Forum 1993;95–98:507–20.
[22] Erdélyi Z, Beke D. J Mater Sci 2011;46:6465–83.